A Neutron Reflectivity Study of Polymer-Modified Phospholipid Monolayers at the Solid-Solution Interface: Polyethylene Glycol-Lipids on Silane-Modified Substrates

T. L. Kuhl,[#] J. Majewski,[*] J. Y. Wong,[#] S. Steinberg,[#] D. E. Leckband,[§] J. N. Israelachvili,[#] and G. S. Smith[*]

[*]Manuel Lujan, Jr. Neutron Scattering Center, Los Alamos National Laboratory, Los Alamos, New Mexico 87545; [#]Department of Chemical Engineering, University of California, Santa Barbara, California 93106; and [§]Department of Chemical Engineering, University of Illinois at Urbana-Champaign, Urbana, Illinois 61801 USA

ABSTRACT   The structure of polymer-decorated phospholipid monolayers at the solid-solution interface was investigated using neutron reflectometry. The monolayers were composed of distearoylphosphatidylethanolamine (DSPE) matrixed with varying amounts of DSPE-PEG (DSPE with polyethylene glycol covalently grafted to its headgroup). Mixed lipid monolayers were Langmuir-Blodgett deposited onto hydrophobic quartz or silicon substrates, previously hydrophobized by chemically grafting a robust monolayer of octadecyltrichlorosilane (OTS). We show that this method results in homogeneous and continuous phospholipid monolayers on the silanated substrates and determine that the grafted PEG chains extend away from the monolayers into the solvent phase as a function of their density, as expected from scaling theories. In addition, ligands were coupled to the end of the PEG chains and selective binding was demonstrated using fluorescence microscopy. Our results demonstrate that these constructs are ideal for further characterization and studies with well-defined monomolecular films.

INTRODUCTION

Because of the small length scale and ubiquitous nature of hydrogen in biological systems, neutrons are particularly suitable for elucidating structural information from phospholipid layers. In the case of substrate-supported bilayers in solution, neutrons can penetrate through the thick substrate and probe the buried membrane-solution interface. Bayerl and co-workers were the first to use specular reflection of neutrons to probe the structure of a substrate-supported dimyristoylphosphatidylcholine (DMPC) bilayer on single-crystal quartz (Johnson et al., 1991). This work was continued with studies on the structure of dipalmitoylphosphatidylcholine/cholesterol (DPPC/cholesterol) bilayers and adsorbed streptavidin protein layers on biotin-functionalized multilayers (Reinl et al., 1992; Schmidt et al., 1992). More recently, pure DPPC bilayers on silicon, combined with atomic force microscopy (AFM) studies, were used to study not only the structure of the adsorbed bilayer, but also its surface coverage and homogeneity (Koenig et al., 1996). Because of the weak adhesion of lipids to quartz or silicon substrates, it has proved difficult to form continuous, homogeneous bilayers on these solid supports. One way to overcome this difficulty is to chemically graft the inner monolayer headgroups to the substrate, thereby presenting a robust hydrophobic layer for subsequent adsorption of the outer monolayer. The most commonly used surfactant for such purposes is octadecyltrichlorosilane (OTS). The OTS layer self-assembles on quartz or silicon substrates by re-acting with surface hydroxyl groups to form covalent siloxy bonds with the substrate (Maoz and Sagiv, 1984). An extensive array of techniques has been used to characterize such OTS layers, including AFM, ellipsometry, x-ray photoelectron spectroscopy, IR spectroscopy, and x-ray and neutron reflectivity (DePalma and Tillman, 1989; Schwartz et al., 1992; Maoz and Sagiv, 1984; Gun et al., 1984; Angst and Simmons, 1991; Hoffmann et al., 1995; Pomerantz et al., 1985; Silberzan et al., 1991; Fragneto et al., 1996). Thomas and co-workers used neutron reflectivity to subsequently characterize the structure of adsorbed $C_{12}E_4$ (tetraethylene glycol monododecyl ether) monolayers on OTS-grafted silicon substrates (Fragneto et al., 1996).

In a similar vein, we have investigated the structure of phospholipid monolayers placed in a controlled manner by Langmuir-Blodgett (LB) deposition on OTS layers grafted to either quartz or silicon substrates. In our system, the outer lipid monolayer was composed of distearoylphosphatidylethanolamine (DSPE) matrixed with various amounts of DSPE-PEG (DSPE with polyethylene glycol covalently bound to the headgroup). The surface density of the PEG polymer chains was controlled by varying the amount of DSPE bearing a PEG chain from 1.3 to 9.0 mol%. Vesicles composed of such lipid mixtures are currently being used in clinical studies as drug delivery vehicles because liposomes covered by a screening PEG layer are "invisible" to the body's immune system and therefore have much longer bloodstream half-lives (Woodle, 1995; Barenholz et al., 1996; Lasic and Martin, 1995; Lasic and Papahadjopoulos, 1996). Furthermore, these so-called Stealth liposomes can be directed to a desired cell type through the use of specific targeting moieties chemically grafted to the ends of the PEG chains (Lee and Low, 1994; Blume et al., 1993; Allen et al., 1995; Wong et al., 1997). Using the specific ligand-receptor

pair of biotin and streptavidin, we demonstrate the selectivity of our substrate-supported lipid monolayers by fluorescence microscopy.

Previously we studied the structure of phospholipid monolayers containing identical amounts of PEG-lipid at the air-water interface, using both x-ray and neutron scattering (Majewski et al., 1997, 1998). Through these studies, we established that the large lateral packing stresses from the bulky polymer chains were relaxed by out-of-plane protrusions rather than an increase in the area per lipid molecule. In the current study, we also probe the factors that affect the entropic fluctuations of phospholipid monolayers at the solid-solution interface.

EXPERIMENTAL SECTION

Materials

DSPE (MW 747) and DMPC (MW 677.9) were purchased from Avanti Polar Lipids (Alabaster, AL), the DSPE-PEG and DSPE-PEG-biotin (MW = 2991) were a generous gift from Sequus Pharmaceuticals (Menlo Park, CA), and OTS was purchased from Fluka (Ronkonkoma, NY). Biotin-X DHPE and Texas Red-DHPE (1,2-dihexadecanoyl-sn-glycero-3-phosphaethanolamine triethylammonium salt) were purchased from Molecular Probes (Eugene, OR). Free biotin was purchased from Calbiochem (La Jolla, CA). Bicyclohexyl from Aldrich Chemicals (St. Louis, MO) was dried by passing through a column of Alumina B (ICN Biomedicals, Eschwege, Germany) just before use. The quartz monocrystalline and silicon substrates were purchased from Atomergic Chemetals Corp. (Farmingdale, NY). D_2O was purchased from Sigma (St. Louis, MO).

Neutron reflectivity

The neutron measurements were made on the SPEAR reflectometer at the Manuel Lujan, Jr. Neutron Scattering Center (MLNSC) at the Los Alamos National Laboratory. The range of neutron wavelengths was 1–16 Å. The measured Q_z range was from 0.008 to ~0.15 Å^{-1}, and reflectivities R with reasonable statistics were obtained to values of $R \approx 10^{-6}$. Typical counting times were 8–9 h. The reflected neutrons were counted with an Ordela model 1202N linear position-sensitive ^{3}He detector. The data were reduced and plotted as $R*Q_z^4$ versus the perpendicular scattering vector, Q_z (this compensates for a sharp Q_z decrease of the reflectivity due to Fresnel's law). The error bars on the data represent the statistical errors in the measurements (standard deviation, σ_R), where the uncertainty in the Q_z resolution, σ_{Q_z}/Q_z, was nearly constant over this scattering vector range with a value of ~3% (Smith et al., 1993). The reflectivity was calculated by the iterative, dynamical method (Russel, 1990). The fits included an additional parameter to normalize the calculated reflectivity to the data. The coherent scattering length densities of the materials used in this work are shown in Table 1 (Sears, 1984).

The reflectivity data were analyzed using the optical matrix method. The various layers (oxide, OTS, phospholipid, etc.) were modeled by boxes of a specified length and scattering length density. Based on this input, a "model" reflectivity profile was generated and compared to the actually measured reflectivity profile. The model was then adjusted to obtain the best least-squares fit to the data. Our philosophy was to use the simplest yet most physically reasonable model to fit the experimental data. We began with one-box models for the bilayer of OTS-phospholipid, adding additional boxes for the polymer and oxide layer on silicon. A single Gaussian roughness was used to smear the interfaces, and the resulting model reflectivity was compared to the data. In all cases, we found that a thickness of ~50 Å was obtained for the OTS-phospholipid bilayer. Although the reflectivity profile and low momentum transfer range were well simulated by this model, the data in the high-momentum transfer

TABLE 1 Scattering length densities of the materials used in this study

Material	Scattering length density, SLD (10^{-6} Å^{-2})
Quartz in air	4.32*
Quartz in D_2O	4.48#
Silicon	2.07
SiO_2 (amorphous)	3.41
H_2O	−0.56
D_2O	6.38
$C_{18}H_{37}$ per 18.5 Å^2	−0.44
$C_{18}H_{37}$ per 23.5 Å^2	−0.35
DSPE headgroup per 42 Å^2	2.66
$(OCH_2CH_2)_n$	0.6

*Measured value.
#We measured a SLD of 1.90×10^{-6} Å^{-2} for quartz relative to D_2O. We assumed that the SLD for D_2O is, as expected, $\beta_{D_2O} = 6.38 \times 10^{-6}$ Å^{-2} and determine the SLD of quartz to be $\beta_{quartz} = 4.48 \times 10^{-6}$ Å^{-2}. Ideally, we should have obtained 4.32×10^{-6} Å^{-2} as was measured in air. We have therefore taken an average value of $\beta_{quartz} = 4.4 \pm 0.1 \times 10^{-6}$ Å^{-2} throughout this work. We do not have a definitive explanation for this discrepancy.

region was not. As such, we began to increase the complexity of our model by adding boxes to account for the various layers of the interfacial film. The results presented in this work are the best fit to the data by the use of simple, insightful models. At all times, we attempted to model our system with physically reasonable values. In particular, we found that when the models were left to run freely (no constraints or fixing of values to a certain range), the fitted scattering length density of the hydrocarbon regions fell below the lowest physically reasonable calculated value of -0.44×10^{-6} Å^{-2} (see Table 1). This trend was found for all of the DSPE-PEG concentrations regardless of substrate. As a result, we found it necessary to confine the scattering length density of the hydrocarbon region to a sensible range of values. Large variations in parameter space were allowed, but we restricted our models to those that generated reasonable results based on the known lengths and scattering length densities of the constituent molecules. Although this made the fitting more difficult, the large number of similar experiments enabled us to fit the data with a high level of self-consistency.

Substrates and OTS layer

Quartz and silicon substrates were used throughout these studies. The substrates were prepared under identical conditions, and one representative quartz and silicon substrate was characterized with neutron reflectivity before construction of the OTS layer. The roughness of the bare quartz substrate was 5.0 ± 0.3 Å and had a scattering length density (SLD) of $\beta_{quartz} = 4.3 \times 10^{-6}$ Å^{-2}. The silicon substrate and native oxide layer were modeled with a uniform 10 ± 5 Å thick box of SLD $\beta_{oxide} = 3.8 \times 10^{-6}$ Å^{-2} and a roughness of 4.0 Å.

Initially, our studies were mainly concerned with characterizing phospholipid monolayers adsorbed to silanated quartz substrates. Instead of doing multiple experiments with different contrasting solvents, i.e., quartz matched water, we duplicated some of our experiments with substrates of different scattering length densities, i.e., quartz versus silicon. In retrospect, varying the contrast of the solvent would have been a wiser choice. The silicon data are more difficult to analyze because the length scale of the native oxide layer (~10 Å) is similar to both the grafted OTS layer as well as the L-B deposited phospholipid monolayer. In the future, growing thicker oxide layers would make the structural analysis easier.

OTS monolayers were assembled on the quartz and silicon surfaces following the procedure of Maoz and Sagiv (1984). The substrates were cleaned with no-chromix and surface hydroxylated by immersion for 5–10

min in a 10 wt% base solution of NaOH at 55°C immediately. The substrates were then thoroughly dried in a stream of clean nitrogen gas and placed in a 1 mM OTS-bicyclohexyl solution for 10–30 min. The OTS-coated substrates were then rinsed in clean chloroform and baked at 100°C for at least 3 h to promote cross-polymerization of the OTS layer.

The quality of the OTS layer was initially determined by contact angle measurements. The contact angles on either the quartz- or silicon-coated monocrystals were remarkably high, 110°, and, significantly, had little or no hysteresis. We believe the exceptional quality of the OTS layers was due in part to the smoothness of our monocrystals, which provided a nearly "perfect" template for chemically grafting the OTS layer. The quality of the OTS layer on one of the silicon substrates was also studied by AFM (Nanoscope III; Digital Instruments, Santa Barbara, CA). A corner of one of the silicon wafers was broken off and characterized. No holes were found, and the roughness of the OTS layer in air was 1.5 ± 0.2 Å over six different 6 μm^2 scans.

Phospholipid monolayer and liquid-solid interface cell

Monolayers of DSPE matrixed with 1.3, 4.5, or 9.0 mol% of DSPE-PEG were LB deposited at a surface pressure of $\Pi = 42$ mN/m (corresponding to a mean area per lipid molecule of ~42 Å^2) on the hydrophobic OTS-coated substrates by being passed down through the air-water interface. At 42 mN/m, the lipid monolayer is in the solid gel phase and is stable over the 8–9 h required for the neutron reflectivity measurements. Our previous studies at the air-water interface of these monolayer compositions indicated that no lateral phase separation occurs in the mixed monolayers and that DSPE and DSPE-PEG mix ideally (Kuhl et al., 1995). In contrast, Sackmann and co-workers found that mixtures of different tail lengths, DMPE and DSPE-PEG, phase separated at low surface pressures (Baekmark et al., 1995). For mixtures of DSPE and DSPE-PEG at surface pressure of 42 mN/m, the PEG chains are in the water subphase and do not penetrate the 2-D plane of the DSPE monolayer. However, the large lateral polymer-polymer repulsive interaction within the subphase does lead to large out-of-plane motions of the lipids at the air-water interface (Majewski et al., 1997, 1998). After the mixed DSPE/DSPE-PEG monolayer was LB deposited on the silanated substrate, the liquid-solid interface cell was assembled under Millipore water, $\Omega = 18$ (Fig. 1). The Millipore water was later exchanged by carefully flushing with D_2O to provide neutron reflectivity contrast. The temperature was maintained at 21°C for both the LB depositions and neutron reflectivity measurements.

Preparation of giant vesicles and flow cell measurements

A solution of DMPC, Texas-Red DHPE (1 mol%) and Biotin-X DHPE (0.16 mol%) was dissolved in a mixture of chloroform:methanol (9:1) and dried overnight on a roughened Teflon disk. Phosphate buffer was gently added to hydrate the lipid film for a few hours at 37°C, creating giant unilamellar vesicles. The vesicle suspension was then further diluted with buffer to obtain a final concentration of 2 mg/ml. A streptavidin solution, 0.05 mg/ml final concentration, was then added to coat the vesicles by binding to the Biotin-X DHPE headgroups (Chiruvolu et al., 1994). In our control experiment to demonstrate specificity, vesicles were not incubated with streptavidin. Vesicles prepared in this manner were quite polydisperse, with an average size of 2 μm, as ascertained by light scattering.

The bilayers used for the fluorescence studies were constructed on circular glass microscope coverslips that were glued to a stainless steel frame before LB deposition. As described above, an OTS inner monolayer was first chemically grafted to the glass surface, after which an outer phospholipid monolayer containing 4.5 mol% DSPE-PEG-biotin was LB deposited on the hydrophobic inner layer. The terminus of the PEG chains was biotinylated and could bind the corresponding receptor streptavidin (Wong et al., 1997; Florin et al., 1994; Leckband et al., 1994). The constructed bilayer was transferred under water into a flow cell as de-
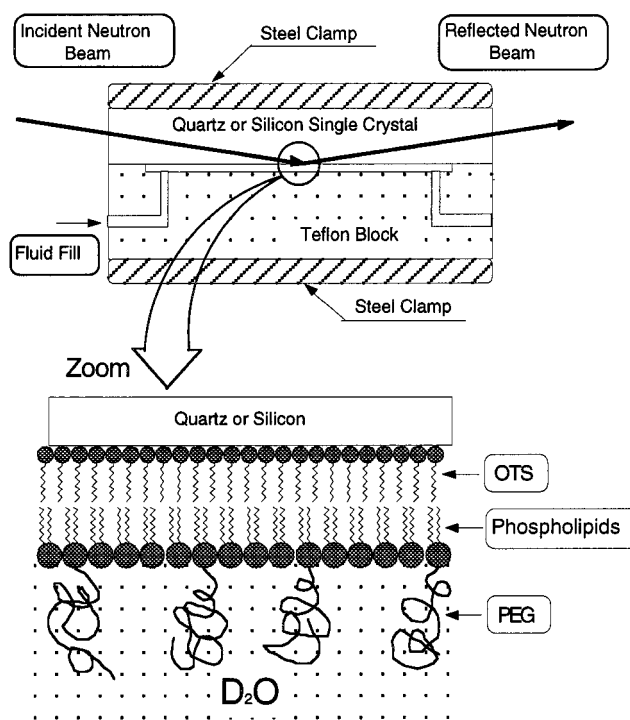

FIGURE 1 Diagram of the liquid-solid interface cell used for neutron reflectivity measurements. The neutron beam travels through the substrate and probes the solid-solution interface, the phospholipid-OTS bilayer submerged in D_2O. The only contacting surfaces in the cell are quartz or silicon and Teflon. The inset shows a schematic representation of the bilayer at the solid-solution interface.

scribed by (Evert et al.) 1994. Afterward, the vesicle suspension was injected into the flow cell. The flow cell had an internal volume of ~1 ml, and solution exchange involved pushing a minimum of 10 ml through the cell at a flow rate of 2 ml/min.

RESULTS

Neutron reflectivity data

OTS monolayers

The chemically grafted OTS monolayers on quartz and silicon were further characterized in air and D_2O by neutron reflectivity. Because the contrast between the substrates and the headgroup of OTS is not very large, we first modeled the OTS layer with a single box and Gaussian roughness. The parameters from such a model are listed in Table 2 for both the quartz and silicon substrates in air. The corresponding fits to the reflectivity curves are shown in Fig. 2. For comparison, fits obtained when the OTS layer was neglected are also shown. As can be seen, although the contrast between the hydrogenated OTS layer and air is not very large, neutron reflectivity is sensitive to the presence of OTS on quartz when the scattering is not dominated by an oxide layer.

The reflectivity profiles in D_2O are much more sensitive to the structure of the OTS layer. Again, we first modeled the OTS layer with a single box and one Gaussian rough-

TABLE 2   Fitting parameters for OTS monolayers in air

Substrate	T_{OTS} (Å)	β_{OTS} ($\times 10^{-6}$ Å^{-2})	T_{oxide} (Å)	β_{oxide} ($\times 10^{-6}$ Å^{-2})	σ (Å)	χ^2
Quartz	24.2 ± 2	-0.4 ± 0.2			5.5 ± 0.2	1.1
Silicon	18.2 ± 2	-0.16 ± 0.1	12.9 ± 2	3.8 ± 0.1	4.0 ± 0.2	8.2

T refers to the thickness of the specified box in ångstroms, β to the scattering length density in Å^{-2} with respect to air, and σ is the Gaussian roughness of the interface.

ness. The parameters from such a model are listed in Table 3; the corresponding fits are shown in Figs. 3 and 4. The thicknesses of the OTS layers were 29 ± 2 Å and 19 ± 2 Å on the quartz and silicon surfaces, respectively. These values may be compared to the length of a fully stretched, methyl terminated C_{18} chain:

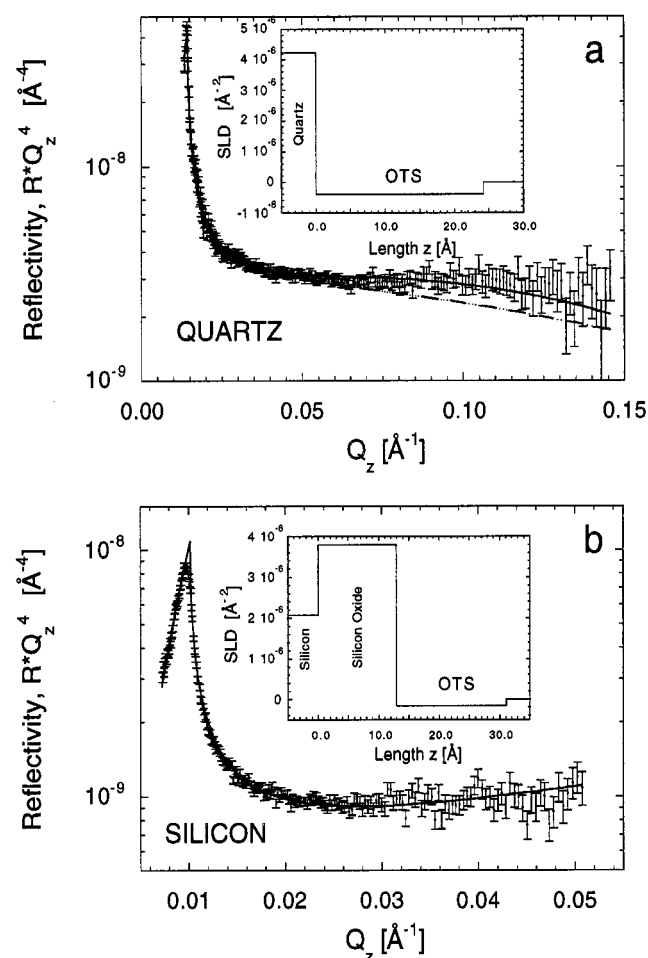$$T_{max} = 1.5 + n \times 1.265 \text{ Å} = 23 \text{ Å} \tag{1}$$

FIGURE 2   Neutron reflectivity data and modeled scattering length density (SLD) profiles at the air-OTS interface of an OTS monolayer chemically grafted to a (*a*) quartz and (*b*) silicon substrate. The solid curves through the data are the fits from a one-box model for the OTS layer on quartz and a two-box model for the OTS and oxide layer on silicon (see *insets*). Although the contrast between OTS and air is small, a surface layer on the quartz substrate was required to fit the reflectivity profiles, as demonstrated by the poor fits (*dashed curve*) obtained when the OTS layers were neglected and the surface roughness was 5.0 Å (*a*). Fitting parameters for the models are given in Table 2.

The model used to fit the reflectivity curves on the quartz substrate was further refined by using two boxes, one for the tail region and another to represent the headgroup of the OTS molecules. For silicon, there is not sufficient contrast between the OTS headgroup and native oxide layer to distinguish between these two layers. Parameters for this more complex model for OTS on quartz are also given in Table 3. The two-box model yields a slightly larger thickness for the OTS layer (tails + heads). Indeed, the total thickness of 31 ± 2 Å on the quartz substrate is actually slightly greater than the 29 Å expected for a fully extended OTS layer normal to the substrate. Both the thickness and scattering length density of $\beta = -0.4$, as compared to air, indicate that an almost perfect and tightly packed OTS layer was self-assembled on the quartz substrate with little or no tilting of the molecules.

It has previously been suggested that OTS may form a "carpet" in which neighboring molecules are cross-polymerized, but that not every OTS molecule forms a bond to the substrate surface (Silberzan et al., 1991). In this manner, the silanated substrate may appear more uniform and less rough. As a further refinement of the model of OTS on quartz, we introduced two different roughnesses for the quartz-OTS and OTS-D$_2$O interfaces, σ_1 and σ_2, respectively. The parameters from such a model are also given in Table 3. Although this model brought the total thickness down slightly to 29 ± 2 Å for the OTS layer, the fit was not quite as good when compared to the results using a single roughness parameter for both interfaces, χ^2 of 1.1 versus 1.5. A lower χ^2 of 1.1 could only be obtained for this model if the thickness of the OTS layer were increased to 33.6 Å, the opposite trend expected for the "carpet" hypothesis.

In contrast, the layer formed on the amorphous silicon substrate was not as thick, 19 ± 2 Å for the hydrocarbon layer compared to 23 Å for an all-trans hydrocarbon chain. Similarly, the measured SLD $\beta = 0.7 \pm 0.1$ for the tail region was higher than expected for a tightly packed hydrocarbon layer. The measured SLD is indicative of a less well packed and/or patchy OTS layer in D$_2$O. Although neutron reflectivity cannot distinguish between these two possibilities, AFM measurements can provide additional information. A typical AFM image is shown in Fig. 5. In general, the images were essentially featureless, with height variations of only 1.5 Å rms. No holes or bare patches were ever detected. Because of the robustness of the chemical grafting of the OTS layer to the substrate, it was not possible to "dig" a hole through the layer with the AFM tip. As a

TABLE 3 Fitting parameters for OTS monolayers in D_2O

	1-Box Model					
Substrate	T_{OTS} (Å)	β_{OTS} ($\times 10^{-6}$ Å^{-2})	T_{oxide} (Å)	β_{oxide} ($\times 10^{-6}$ Å^{-2})	σ (Å)	χ^2
Quartz	29 ± 2	-0.4 ± 0.1			4.0 ± 0.2	1.1
Silicon	19 ± 2	0.7 ± 0.1	7.7 ± 2	3.8 ± 0.1	4.1 ± 0.2	2.8
	2-Box Model					
	$T_{OTS\ tails}$ (Å)	$\beta_{OTS\ tails}$ ($\times 10^{-6}$ Å^{-2})	$T_{OTS\ heads}$ (Å)	$\beta_{OTS\ heads}$ ($\times 10^{-6}$ Å^{-2})		
Quartz	23.7 ± 1	-0.4 ± 0.1	7.6 ± 1	1.1 ± 0.1	3.4 ± 0.2	1.1
					σ_1 $\qquad$ σ_2	
Quartz	23.0 ± 1	-0.4 ± 0.1	6.0 ± 1	1.1 ± 0.1	5.0 $\qquad$ 3.8	1.5

T refers to the thickness of the specified box in ångstroms, β to the scattering length density in Å^{-2} with respect to air, and σ is the Gaussian roughness of the interface. The SLDs were converted to their values relative to air by adding the SLD of the substrate to the measured values. For quartz we measured a value of $4.4 \pm 0.1 \times 10^{-6}$ Å^{-2}, whereas for silicon we obtained a value of $2.1 \pm 0.1 \times 10^{-6}$ Å^{-2}.

result, we were unable to determine the thickness of the OTS layer on silicon with this technique. Although AFM and neutron reflectivity sample different length scales (μm^2 versus cm^2), the homogeneity of the OTS layer measured

with AFM implies that a continuous OTS layer was assembled on the silicon substrate. The thickness of 19 Å, as measured by neutron reflectivity, can then be used to determine the tilt of the hydrocarbon tails in the monolayer by
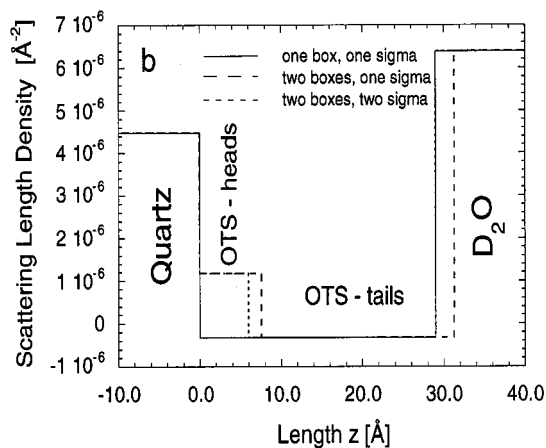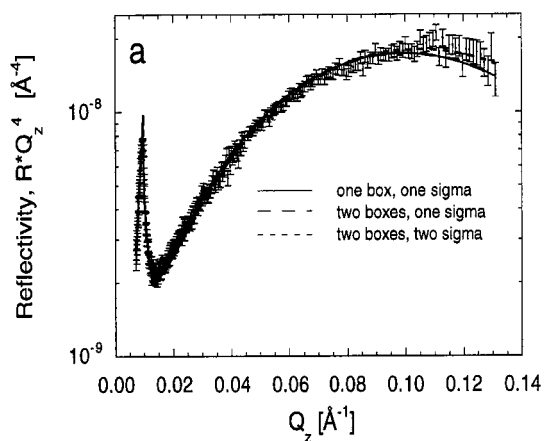

FIGURE 3 (*a*) Neutron reflectivity data at the D_2O-quartz interface of an OTS monolayer chemically grafted to the quartz substrate. The curves (almost superimposed) through the data are the fits from a one-box and a two-box model. (*b*) Corresponding scattering length density profiles of the one-box and two-box models. Fitting parameters for the models are given in Table 3.
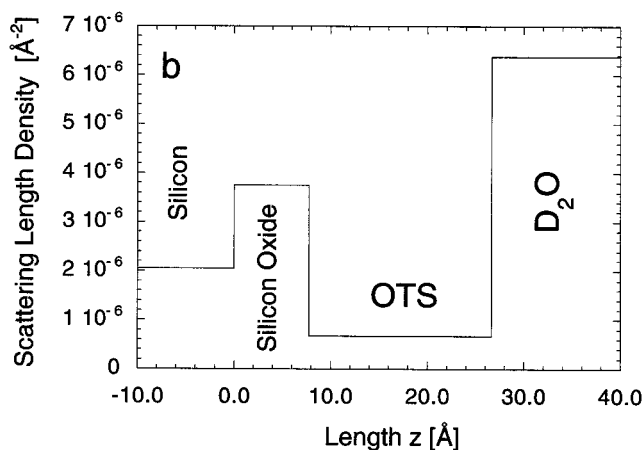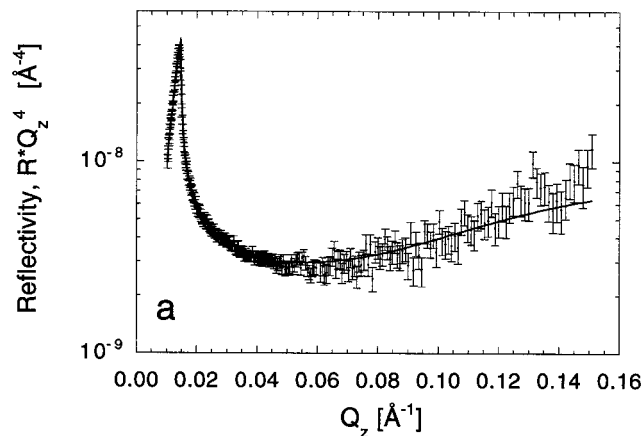
FIGURE 4 (*a*) Neutron reflectivity data at the D_2O-silicon interface of an OTS monolayer chemically grafted to the silicon substrate. The solid curve is a fit using a two-box model, one for the OTS layer and one for the native oxide layer. (*b*) Corresponding scattering length density profiles of the one-box model. Fitting parameters for the model are given in Table 3.

FIGURE 5 AFM image of OTS on a silicon substrate used in the neutron reflectivity studies. No holes or patches were detected in any scans. The underlying terraced pattern is due to a slight miscut angle (less than 0.05°) when the substrate was prepared by the manufacturer.
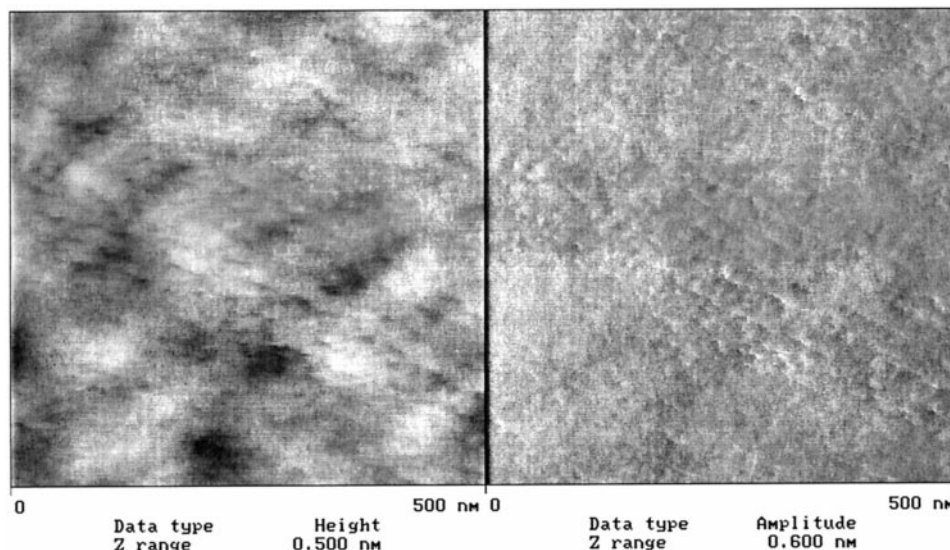
using

$$\cos^{-1} \theta = \frac{T_{\text{fit}}}{T_{\text{max}}} \left(\frac{180}{\pi}\right) = 34° \qquad (2)$$

This tilt also indicates that there is an increased area per OTS molecule. Likewise, the measured SLD of $\beta = 0.7 \pm 0.1$ in D_2O for the tail region might be higher than expected because this layer contains some heavy water molecules. In fact, the number of water molecules with SLD β_{D2O} contained within this layer can be calculated using

$$\beta_{\text{measured}} = \phi\beta_{\text{hydrocarbon}} + (1 - \phi)\beta_{D_2O} \qquad (3)$$

where ϕ is the volume fraction of hydrocarbon material of SLD $\beta_{\text{hydrocarbon}}$. Equation 3 can be rewritten in terms of the scattering lengths b of the hydrocarbon chains and water, number of water molecules n and total volume per OTS molecule V_{total}:

$$\beta_{\text{measured}} = \frac{b_{\text{hydrocarbon}} + nb_{\text{water}}}{V_{\text{total}}} \qquad (4)$$

where

$$V_{\text{total}} = AT_{\text{measured}} = V_{\text{material}} + nV_{\text{water}} = \phi AT_{\text{measured}} + nV_{\text{water}} \qquad (5)$$

Solving for A and n, we calculate an area of 23.5 Å^2 and 2.9 waters per OTS molecule. In comparison, the OTS molecule on the quartz substrate is tightly packed, with an area less than 20 Å^2, and no water was detected in the OTS layer. Finally, although the microscopic structures of the OTS monolayer on quartz and silicon were quite different, the macroscopic contact angles were indistinguishable at $\theta = 110°$.

Phospholipid monolayers on solid supports

Silanated quartz substrates

Next the structure of phospholipid monolayers LB deposited on the silanated quartz was investigated. The phospholipid monolayers were composed of DSPE matrixed with 1.3, 4.5, or 9.0% DSPE-PEG. The measured reflectivity profiles are shown in Fig. 6. The peaks in the reflectivity curves are due to the thickness of the lipid-OTS bilayers on the substrates. The position of the maximum $Q_{z(peak)}$ in reciprocal space Q_z can be used to calculate the approximate thickness of the bilayer directly from (Russell, 1990)

$$T_{\text{bilayer}} = \frac{\pi}{Q_{z(peak)}} \qquad (6)$$

Using this expression, the thickness of the bilayer on quartz is ~52 Å for all compositions of DSPE/DSPE-PEG, whereas that on silicon is ~48 Å. The difference of 4 Å most likely corresponds to the difference in thickness of the OTS layers on quartz and silicon.

We next modeled the lipid layer with two boxes, one for the headgroup region, the other for the tail region. The polymer layer was modeled with either a step function (one box) or a parabolic density gradient (Alexander, 1977; de Gennes, 1980; Milner et al., 1988; Szleifer and Carignano, 1996). It was not possible to obtain a reasonable fit to the highest polymer concentration (9.0%) of DSPE-PEG using a step function. At this high concentration, the polymer layer is expected to have a parabolic density gradient, and such a model for the polymer layer indeed gives a much better fit to the reflectivity data, although we cannot rule out different, more complicated models (Majewski et al., 1997). Similarly, the fit to the 4.5% DSPE-PEG data was slightly better when we used this functional form. For ease of comparison, the 1.3% data were modeled in the same way, although the fit was not sensitive to the form of the profile
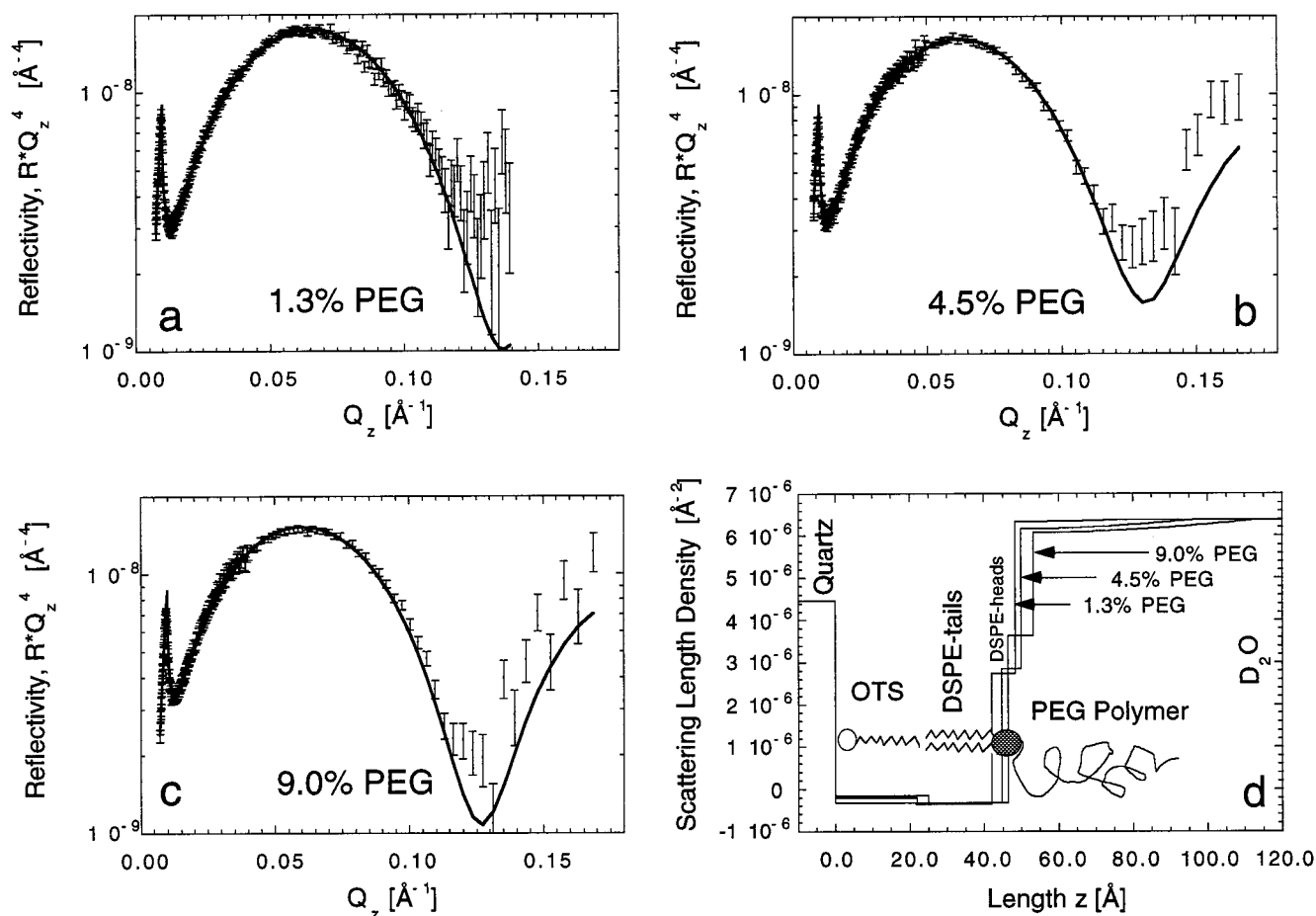
FIGURE 6　Neutron reflectivity data of mixed DSPE/DSPE-PEG monolayers on silanated quartz substrates. (*a*) 1.3% DSPE-PEG. (*b*) 4.5% DSPE-PEG. (*c*) 9.0% DSPE-PEG. The data are fit using box models for the lipid and OTS layers and a parabola for the extended polymer layer. Parameter values are listed in Table 4. (*d*) Corresponding scattering length density profile of the model, including the positions of the constituent molecules.

at this low polymer concentration. The parameter values on quartz are given in Table 4, and reflectivity fits are shown in Fig. 6.

The roughness of the phospholipid-OTS bilayer was modeled as a Gaussian and broken down into two components. σ_1 corresponds to the roughness of the quartz substrate, and σ_2 corresponds to the roughness of the rest of the interfaces between the boxes used to model the various layers of different thicknesses and SLDs. When we used only a single roughness factor for both interfaces, we obtained a value of 2.1 ± 0.4 Å. This is much less than the 5.0 and 3.4 Å measured for the bare and OTS grafted quartz substrates (Table 3). Indeed, for both the single and two sigma models, the apparent roughness of the phospholipid

monolayer is reduced compared to the bare substrate. In addition, when a single Gaussian roughness was used, the SLDs obtained for the lipid and OTS hydrocarbon tail regions were -1.0×10^{-6} Å^{-2} and -0.8×10^{-6} Å^{-2}, respectively, compared to air. These values are physically unreasonable compared to the theoretical SLD of -0.4×10^{-6} Å^{-2} for tightly packed hydrocarbon chains (Table 1).

Finally, the OTS-lipid bilayer remains relatively constant with a thickness of 52 ± 2 Å, whereas the length and depth of the polymer layer increase with increasing DSPE-PEG concentration (due to the displacement of highly scattering D$_2$O by the poorly scattering hydrogenated PEG layer). We had anticipated some roughening of the lipid monolayer due to the bulky polymer headgroups, but this was not borne

TABLE 4　Parameters from fits to the phospholipid monolayer on OTS grafted quartz substrates

DSPE-PEG (mol%)	σ_1 (Å)	σ_2 (Å)	$T_{\text{lipid heads}}$ (Å)	$\beta_{\text{lipid heads}}$ ($\times 10^{-6}$ Å^{-2})	$T_{\text{lipid tails}}$ (Å)	$\beta_{\text{lipid tails}}$ ($\times 10^{-6}$ Å^{-2})	T_{OTS} (Å)	β_{OTS} ($\times 10^{-6}$ Å^{-2})	T_{parabola} (Å)	β_{parabola} ($\times 10^{-6}$ Å^{-2})	χ^2
1.3	5.9	1.0	6.3 ± 1	2.7 ± 0.2	20.6 ± 2	-0.4 ± 0.1	21.5 ± 2	-0.4 ± 0.1	25 ± 10	6.29 ± 0.05	2.0
4.5	7.1	1.0	5.3	2.8	22.7	-0.4	21.9	-0.3	46 ± 5	6.12	1.2
9.0	6.3	1.2	6.8	3.6	21.4	-0.4	25.1	-0.2	59 ± 5	6.03	1.8

The fitted SLDs were converted to their values relative to air by adding the SLD of quartz, $4.4 \pm 0.1 \times 10^{-6}$ Å^{-2}.

TABLE 5 Parameters from fits to the phospholipid monolayer on OTS grafted silicon substrates

DSPE-PEG (mol%)	σ_1 (Å)	σ_2 (Å)	$T_{\text{lipid heads}}$ (Å)	$\beta_{\text{lipid heads}}$ ($\times 10^{-6}$ Å^{-2})	$T_{\text{lipid tails}}$ (Å)	$\beta_{\text{lipid tails}}$ ($\times 10^{-6}$ Å^{-2})	T_{OTS} (Å)	β_{OTS} ($\times 10^{-6}$ Å^{-2})	T_{parabola} (Å)	β_{parabola} ($\times 10^{-6}$ Å^{-2})	χ^2
1.3	4.2	1.7	7.2 ± 1.5	2.9 ± 0.1	24.2 ± 2	−0.4 ± 0.1	20.0 ± 2	0.3 ± 0.1	30 ± 10	6.2	12.5
4.5	6.8	2.0	7.1	3.1	25.7	−0.1	20.1	0.4	50 ± 5	5.6	9.3

The fitted SLDs were converted to their values relative to air by adding the SLD of silicon, $2.1 \pm 0.1 \times 10^{-6}$ Å^{-2}.

out. A well-packed lipid monolayer remained deposited on the silanated quartz substrate.

Silanated silicon substrates

The parameter values and resulting reflectivity fits for the DSPE/DSPE-PEG monolayers on silicon are shown in Table 5 and Fig. 7. Even though the quality of the grafted OTS layer formed on silicon was not as good as that formed on quartz, the monolayer deposited on this surface was very similar to that measured on quartz. The SLD for the lipid hydrocarbon tails of -0.4 ± 0.1 relative to air ($-2.5 +$

2.1 × 10^{-6} Å^{-2}) is again that expected for a tightly packed area per tail of 20 Å^2. Similarly, the thicknesses obtained for the lipid head, lipid tail, and polymer layers are also very close. These measurements indicate that the structure of the LB deposited lipid layer was not greatly affected by the underlying structure of the OTS layer. We again modeled the polymer layer with a parabolic density distribution and found that the length and depth of the parabola increased with increasing DSPE-PEG concentration in the lipid monolayer. At the lower concentration of 1.3% DSPE-PEG, we were not sensitive to the form of the density distribution, but at 4.5% DSPE-PEG a parabolic profile fit the data better than a step function.

In summary, these neutron scattering results indicate that well-formed lipid monolayers were deposited on the silanated substrates and that a polymer layer was extending into the aqueous phase as a function of the DSPE-PEG concentration. We next used fluorescence microscopy to confirm the structure on a more macroscopic level.

Fluorescence microscopy

The ability to selectively bind desired biological objects by extended polymer chains was demonstrated using fluorescence microscopy. As described in the Materials section, 4.5% DSPE-PEG with biotin moieties at the PEG terminus was LB deposited on silanated glass coverslips. (Although biotin was chosen for these studies, other targeting moieties or "ligands" can be end-grafted to PEG chains, and a wide range of specific binding systems or associations can thus be made in a similar fashion; Zalipsky, 1995; Zalipsky et al., 1996.) After assembly of the flow cell, 1 ml of fluorescently labeled liposomes bearing biotin's receptor, streptavidin, was injected into the fluid chamber (Evert et al., 1994). Binding of these liposomes was evident within minutes of the injection. As shown in Fig. 8 *a*, after 4 h a significant quantity of targeted liposomes bound to the surface. Moreover, these bound liposomes could be partially removed by incubation with soluble biotin, which has a higher binding affinity for streptavidin than PEG-biotin (Fig. 8 *c*). In addition, adsorption was completely absent when the liposomes were not incubated with streptavidin (Fig. 8 *b*).
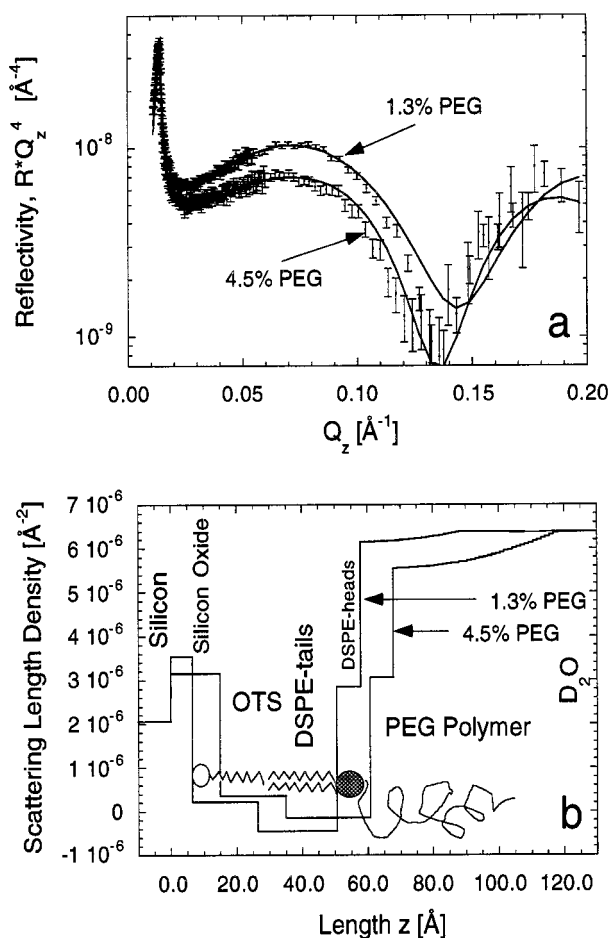
FIGURE 7 (*a*) Neutron reflectivity data of mixed DSPE/DSPE-PEG monolayers on silanated silicon substrates. The data are fit using box models for the lipid and OTS layers and a parabola for the extended polymer layer. Parameter values are listed in Table 5. (*b*) Corresponding scattering length density profile of the model, including the positions of the constituent molecules.

DISCUSSION

By examining the results in Figs. 3 and 4 and Table 3, we can make several observations regarding the OTS monolayer structure. First, we see that the values obtained in this

FIGURE 8 Typical fluorescent images of selective binding of vesicles to an LB deposited 4.5% DSPE-PEG-biotin monolayer at the solid-solution interface after 4 h of incubation (*a*). The lack of fluorescence in *b* indicates that little or no nonspecific adsorption of vesicles occurs in the absence of streptavidin under the same conditions as in *a*. (*c*) Release of previously bound vesicles by incubation with free biotin. Soluble biotin has a significantly higher binding affinity for streptavidin and competes effectively with and eventually replaces the original bound ligand (Chiruvolu et al., 1994; Leckband et al., 1994). All images shown are from a continuous experiment.
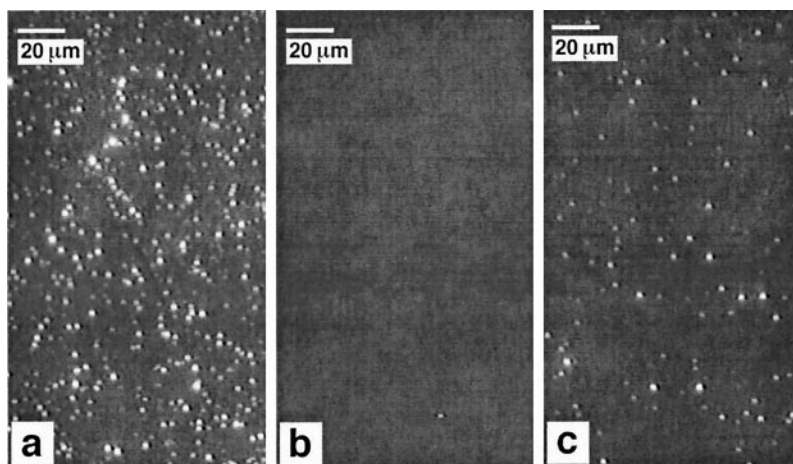
study are consistent with those previously measured with x-rays and neutrons for OTS monolayers on silicon (Pomerantz et al., 1985; Wasserman et al., 1989; Silberzan et al., 1991; Fragneto et al., 1996). From these x-ray studies, reported values for the OTS head and tail lengths normal to the substrate were 5.6 Å and from 16.3 to 23 Å, respectively. Satija and co-workers, using neutron reflectivity, reported thicknesses ranging from 11 to 24 Å for the tail region, depending on the surface coverage for the OTS layer on silicon (Fragneto et al., 1996). In this study the values were 7.0 ± 1 and 23.7 ± 1 Å on quartz, and a hydrocarbon tail thickness of 19 ± 2 Å on silicon. Our longer tail thickness on quartz is consistent with the expected length for a fully stretched, untilted C_{18} hydrocarbon chain, indicative of a very homogeneous, well-packed OTS monolayer. On silicon, a less dense OTS layer was formed with a calculated average tilt angle of $\theta = 34°$ and approximately three waters per OTS molecule in an area of 23.5 Å^2 (when measured in contact with D_2O). However, neutron reflectivity cannot distinguish between water molecules penetrating within a continuous OTS monolayer versus a patchy or defective OTS layer of 86% coverage on silicon, which is also consistent with our measurements of the SLD for this layer.

The quality of the OTS layer did not seem to have a strong effect on the structure of the LB deposited lipid layer. Similar values for the SLDs relative to air and thicknesses were obtained on both types of substrate. Essentially, a well-packed lipid monolayer could be easily deposited on this now generic "hydrophobic substrate." Moreover, this outer lipid monolayer could be easily removed or stripped off by passing the substrate out through the air-water interface. In fact, throughout these experiments, we reused the same OTS-coated quartz and silicon substrates. To ensure that all residual lipid was removed between experiments, the substrates were rinsed with chloroform.

The surface roughness σ or σ_2 of the lipid monolayers was less than that measured for the bare substrates. The proximity and hydrophobic anchoring to the solid support evidently suppress out-of-plane fluctuations of the mole-

cules ($T < T_c = 56°C$). (However, there is a trend toward slightly increasing bilayer thickness with increasing PEG-lipid concentration.) This is in contrast to our previous studies at the air-water interface, where the roughness and thickness of the monolayer increased dramatically as a function of PEG-lipid concentration due to protrusions out of the monolayer plane (Majewski et al., 1997).

In terms of modeling the density distribution of the PEG segments away from the membrane surface, the most obvious difference between the three concentrations studied, 1.3, 4.5, and 9.0 mol% PEG-lipid, is the increase in the width and depth of the parabola representing the polymer thickness with increasing PEG-lipid concentration (Tables 4 and 5) as the lower scattering polymer ($\beta = 0.6 \times 10^{-6}$ Å^{-2}) displaces D_2O ($\beta = 6.4 \times 10^{-6}$ Å^{-2}). The fitted scattering length densities of the parabolas as a function of DSPE-PEG content can be compared by integrating over the length of the parabola. The integration enables us to compare the total amount of polymer for each of the three DSPE-PEG concentrations on quartz, where the ratios were compared, i.e., 1.3 *versus* 9.0 and 4.5 *versus* 9.0. Our measured ratios are 0.06 and 0.50 compared to the calculated ratios of 0.14 and 0.50 for 1.3 and 4.5 to 9.0% DSPE-PEG, respectively, on quartz. As can be seen, we are less sensitive to the presence of polymer at the lower concentration of 1.3% DSPE-PEG. In addition, the thickness of the polymer layer (parabola) determined by neutron reflectivity matches well with the thickness determined with other techniques, as shown in Table 6.

Finally, part of the usefulness of this system lies in the ability to graft biologically interesting functional groups to the ends of the PEG chains. The grafting density of a targeting ligand can be quantitatively controlled by simply varying its concentration in the Langmuir monolayer, and a host of targeting moieties have already been synthesized for these purposes (Zalipsky, 1995; Zalipsky et al., 1996). We used fluorescence microscopy to demonstrate this effect with biotin moieties and streptavidin-coated vesicles (Fig. 8). Moreover, the substrates used in those studies were rough glass coverslips as opposed to the specially polished,

TABLE 6 Comparison of measured polymer thickness by various techniques

DSPE-PEG (mol%)	Quartz $T_{parabola}$ (Å)	Silicon $T_{parabola}$ (Å)	SFA 1[*] (Å)	SFA 2[#] (Å)	X-ray[§] (Å)	X-ray[¶] (Å)	Neutron[‖] (Å)
1.3%	25 ± 10	30 ± 10	35	35	42	34.8	45
4.5%	46 ± 5	50 ± 5	40	38	52		60
9.0%	59 ± 5		70	50	60	48	75

[*]Kuhl et al. (1994).
[#]Sheth and Leckband (1997).
[§]Kenworthy et al. (1995).
[¶]Majewski et al. (1998).
[‖]Majewski et al. (1997).

extremely smooth quartz and silicon substrates used in the neutron scattering studies. Again, we were able to form a homogeneous lipid monolayer on the solid support, which makes these constructs ideal for characterization studies.

CONCLUSIONS

Data from neutron reflectivity studies of phospholipid monolayers at the solid-solution interface have been presented. Continuous and tightly packed lipid monolayers were deposited on silanated quartz and silicon substrates. Thickness fluctuations of the monolayers were greatly reduced by proximity to and interaction with the solid supports. DSPE-PEG could be incorporated into the monolayer and the polymer chains extended away from the monolayer into the solution. The thickness and density of the polymer layer were varied by simply increasing or decreasing the amount of DSPE-PEG in the monolayer. Finally, targeting moieties could be coupled to the ends of the extending PEG chains, and selective binding was demonstrated.

REFERENCES

Alexsander, S. 1977. Adsorption of chain molecules with a polar head. A scaling description. *J. Phys. Paris.* 38:983–987.

Allen, T. M., E. Brandeis, C. B. Hansen, G. Y. Kao, and S. Zalipsky. 1995. A new strategy for attachment of antibodies to sterically stabilized liposomes resulting in efficient targeting to cancer cells. *Biochim. Biophys. Acta.* 1237:99–108.

Angst, D. L., and G. W. Simmons. 1991. Moisture absorption characteristics of organosiloxane self-assembled monolayers. *Langmuir.* 7:2236–2242.

Baekmark, T. R., G. Elender, D. D. Lasic, and E. Sackmann. 1995. Conformation transitions of mixed monolayers of phospholipids and poly(ethylene oxide) lipopolymers and interaction forces with solid surfaces. *Langmuir.* 11:3975–3987.

Barenholz, Y., E. Bolotin, R. Cohen, and A. Gabizon. 1996. Sterically stabilized doxorubicin loaded liposomes (DOX-SL(TM))—from basics to the clinics. *Phosphorous Sulfer Silicon Related Elements.* 110:293–296.

Blume, G., G. Cevc, M. D. J. A. Crommelin, I. A. J. M. Bakker-Woudenberg, C. Kluft, and G. Storm. 1993. Specific targeting with poly(ethylene glycol)-modified liposomes: coupling of homing devices to the ends of the polymeric chains combines effective target binding with long circulation times. *Biochim. Biophys. Acta.* 1149:180–184.

Chiruvolu, S., S. Walker, J. Israelachvili, F.-J. Schmitt, D. Lecknand, and J. A. Zasadzinski. 1994. Higher order self-assembly of vesicles by site-specific binding. *Science.* 264:1753–1756.

de Gennes, P. G. 1980. Conformations of polymers attached to an interface. *Macromolecules.* 13:1069–1075.

DePalma, V., and N. Tillman. 1989. Friction and wear of self-assembled trichlorosilane monolayer films on silicon. *Langmuir.* 5:868–872.

Evert, L. L., D. Leckband, and J. N. Israelachvili. 1994. Structure and dynamics of ion-induced domains in free and supported monolayers and bilayers. *Langmuir.* 10:303–315.

Florin, E.-L., V. T. Moy, and H. E. Gaub. 1994. Adhesion forces between individual ligand-receptor pairs. *Science.* 264:415–417.

Fragneto, G., L. R. Lu, D. C. McDermott, R. K. Thomas, A. R. Rennie, P. D. Gallagher, and S. K. Satija. 1996. Structure of monolayers of tetraethylene glycol monododecyl ether adsorbed on self-assembled monolayers on silicon: a neutron reflectivity study. *Langmuir.* 12:477–486.

Gun, J., R. Iscovici, and J. Sagiv. 1984. On the formation and structure of self-assembling monolayers. II. A comparative study of Langmuir-Blodgett and adsorbed films using ellipsometry and IR reflection-adsorption spectroscopy. *J. Colloid Interface Sci.* 101:201–213.

Hoffmann, H., U. Mayer, and A. Krischanitz. 1995. Structure of alkylsiloxane monolayers on silicon surfaces investigated by external reflection infrared spectroscopy. *Langmuir.* 11:1304–1312.

Johnson, S., T. M. Bayerl, D. C. McDermott, G. W. Adam, A. R. Rennie, R. K. Thomas, and E. Sackmann. 1991. Structure of an adsorbed dimyristoylphosphatidylcholine bilayer measured with specular reflection of neutrons. *Biophys. J.* 59:289–294.

Kenworthy, K., K. Hristova, D. Needham, and T. J. McIntosh. 1995. Range and magnitude of the steric pressure between bilayers containing phospholipids with covalently attached poly(ethylene glycol). *Biophys. J.* 68:1921–1936.

Koenig, B. W., S. Krueger, W. J. Orts, C. F. Majkrzak, N. F. Berk, J. V. Silverton, and K. Gawrisch. 1996. Neutron reflectivity and atomic force microscopy studies of a lipid bilayer in water adsorbed to the surface of a silicon single crystal. *Langmuir.* 12:1343–1350.

Kuhl, T., D. Leckband, D. Lasic, and J. Israelachvili. 1994a. Modulation of interaction forces between bilayers exposing short-chained ethylene oxide headgroups. *Biophys. J.* 66:1479–1488.

Kuhl, T., D. Leckband, D. Lasic, and J. Israelachvili. 1994b. Modulation and modeling of interaction forces between bilayers exposing terminally grafted polymer chains. *In* Stealth Liposomes. D. Lasic and F. Martin, editors. CRC Press, Boca Raton, FL. 73–91.

Lasic, D., and F. Martin. 1995. Stealth Liposomes. CRC Press, Boca Raton, FL.

Lasic, D. D., and D. Papahadjopoulos. 1996. Liposomes and biopolymers in drug and gene delivery. *Curr. Opin. Solid State Mater. Sci.* 1:392–400.

Leckband, D. E., F.-J. Schmitt, J. N. Israelachvili, and W. Knoll. 1994. direct force measurements of specific and nonspecific protein interactions. *Biochemistry.* 33:4611–4624.

Lee, R. J., and P. S. Low. 1994. Delivery of liposomes into cultured KB cells via folate receptor-mediated endocytosis. *J. Biol. Chem.* 269:3198–3204.

Majewski, J., T. L. Kuhl, M. Gerstenberg, J. N. Israelachvili, and G. S. Smith. 1997. The structure of phospholipid monolayers containing polyethylene glycol lipids at the air-water interface. *J. Phys. Chem.* 101:3122–3129.

Majewski, J., T. L. Kuhl, K. Kjaer, M. C. Gerstenberg, J. Als-Nielsen, J. N. Israelachvili, and G. S. Smith. 1998. An x-ray synchrotron study of packing and protrusions of polymer lipid monolayers at the air-water interface. *J. Am. Chem. Soc.* 120:1469–1473.

Milner, S., T. Witten, and M. Cates. 1988. Theory of grafted polymer brush. *Macromolecules.* 21:2610–2618.

Moaz, R., and J. Sagiv. 1984. On the formation and structure of self-assembling monolayers. I. A comparative ATR-wettability study of Langmuir-Blodgett and adsorbed films on flat substrates and glass microbeads. *J. Colloid Interface Sci.* 100:465–496.

Pomerantz, M., A. Segmuller, L. Netzer, and J. Sagiv. 1985. Coverage of Si substrates by self-assembling monolayers and multilayers as measured by IR, wettability and x-ray diffraction. *Thin Solid Films.* 132:153–162.

Reinl, H., T. Brumm, and T. M. Bayerl. 1992. Changes of the physical properties of the liquid-ordered phase with temperature in binary mixtures of DPPC with cholesterol: a ^{2}H-NMR, FT-IR, DSC, and neutron scattering study.

Russel, T. P. 1990. X-ray and neutron reflectivity for the investigation of polymers. *Mater. Sci. Rep.* 5:171–271.

Schmidt, A., J. Spinke, T. Bayerl, E. Sackmann, and W. Knoll. 1992. Streptavidin binding to biotinylated lipid layers on solid supports: a neutron reflection and surface plasmon optical study. *Biophys. J.* 63:1185–1192.

Schwartz, D. K., S. Steinberg, J. Israelachvili, and J. A. N. Zawadzinski. 1992. Growth of a self-assembled monolayer by fractal aggregation. *Phys. Rev. Lett.* 69:3354–3357.

Sears, V. F. 1984. Thermal-Neutron Scattering Lengths and Cross Sections for Condensed-Matter Research. Atomic Energy Canada Ltd., Chalk River, Ontario, Canada.

Sheth, S. R., and D. Leckband. 1997. Measurements of attractive forces between proteins and end-grafted poly(ethylene glycol) chains. *Proc. Natl. Acad. Sci. USA.* 94:8399–8404.

Silberzan, P., L. Leger, D. Ausserre, and J. J. Benattar. 1991. Silanation of silica surfaces. A new method of constructing pure or mixed monolayers. *Langmuir.* 7:1647–1651.

Smith, G. S., R. Pynn, S. Baker, M. Fitzsimmons, and L. Xuan. 1993. Reflections from LANSCE. *Los Alamos Neutron Scattering Center News Lett.* no. 15 (Spring).

Szleifer, I., and M. A. Carignano. 1996. Tethered polymer layers. *In* Advances in Chemical Physics, Vol. 94. I. Prigogine and S. A. Rice, editors. John Wiley and Sons, New York. 165–259.

Wasserman, S. R., G. M. Whitesides, I. M. Tidswell, B. M. Ocko, P. S. Pershan, and J. D. Axe. 1989. The structure of self-assembled monolayers of alkylsiloxanes on silicon: a comparison of results from ellipsometry and low-angle x-ray reflectivity. *J. Am. Chem. Soc.* 111:5852–5861.

Wong, J. Y., T. L. Kuhl, J. N. Israelachvili, N. Mullah, and S. Zalipsky. 1997. Direct measurement of a tethered ligand-receptor interaction potential. *Science.* 275:820–822.

Woodle, M. C. 1995. Sterically stabilized liposome therapeutics. *Adv. Drug Delivery Rev.* 16:249–265.

Zalipsky, S. 1995. Chemistry of polyethylene glycol conjugates with biologically active molecules. *Adv. Drug Delivery Rev.* 16:157–182.

Zalipsky, S., C. B. Hansen, D. E. Lopes de Menezes, and T. M. Allen. 1996. Long-circulating, polyethylene glycol-grafted immunoliposomes. *J. Controlled Release.* 39:153–161.